

# LEGO-SLAM: Language-Embedded Gaussian Optimization SLAM

Sibaek Lee<sup>✉</sup>, Seongbo Ha<sup>✉</sup>, Kyeongsu Kang<sup>✉</sup>, Joonyeol Choi<sup>✉</sup>, Seungjun Tak<sup>✉</sup>, and Hyeonwoo Yu<sup>✉</sup>

Sungkyunkwan University, South Korea  
 {lmj1ss, sobo3607, thithin0821, joonyeol99, tmdwns8840, hwyu}@g.skku.edu

**Abstract.** Recent advances in 3D Gaussian Splatting (3DGS) have enabled Simultaneous Localization and Mapping (SLAM) systems to build photorealistic maps. However, these maps lack the open-vocabulary semantic understanding required for advanced robotic interaction. Integrating language features into SLAM remains a significant challenge, as storing high-dimensional features demands excessive memory and rendering overhead, while existing methods with static models lack adaptability for novel environments. To address these limitations, we propose LEGO-SLAM (Language-Embedded Gaussian Optimization SLAM), the first framework to achieve real-time, open-vocabulary mapping within a 3DGS-based SLAM system. At the core of our method is a scene-adaptive encoder-decoder that distills high-dimensional language embeddings into a compact 16-dimensional feature space. This design reduces the memory per Gaussian and accelerates rendering, enabling real-time performance. Unlike static approaches, our encoder adapts online to unseen scenes. These compact features also enable a language-guided pruning strategy that identifies semantic redundancy, reducing the map’s Gaussian count by over 60% while maintaining rendering quality. Furthermore, we introduce a language-based loop detection approach that reuses these mapping features, eliminating the need for a separate detection model. Extensive experiments demonstrate that LEGO-SLAM achieves competitive mapping quality and tracking accuracy, all while providing open-vocabulary capabilities at 15 FPS. Our project page is at: <https://lab-of-ai-and-robotics.github.io/LEGO-SLAM/>

**Keywords:** Open-Vocabulary SLAM · 3D Gaussian Splatting

## 1 Introduction

While the foundational objective of Simultaneous Localization and Mapping (SLAM) has long been to jointly construct a map and estimate an agent’s location, technological advancements have elevated the ambition towards generating rich and scalable environmental representations. In response, recent breakthroughs in 3D reconstruction have enhanced the mapping component of SLAM, with Neural Radiance Fields (NeRF) [23] and 3D Gaussian Splatting (3DGS) [12] emerging as prominent solutions for creating photo-realistic maps [37]. NeRF

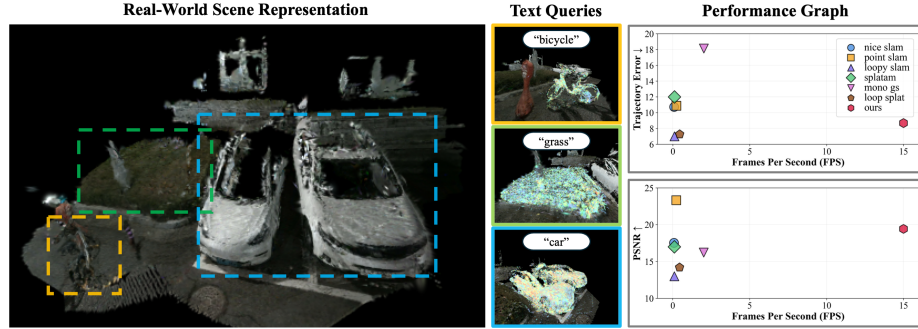


**Fig. 1: LEGO-SLAM: real-time, open-vocabulary 3DGS-SLAM.** (Left) A large-scale real-world scene reconstructed by our system, with colored boxes highlighting specific regions. (Middle) Relevancy maps showing the 3D localization for corresponding text queries. (Right) Graphs on the ScanNet dataset show LEGO-SLAM operates at 15 FPS while maintaining competitive performance.

provided memory-efficient implicit mapping but failed to meet the real-time demands of SLAM due to slow rendering. This limitation was overcome by 3DGS, which delivers high-fidelity mapping at real-time. However, such photorealistic maps lack the semantic understanding required for enabling embodied AI to perform diverse downstream tasks [10, 15, 32, 33]. The evolution of these methods has progressed beyond simple RGB representation to semantic mapping, assigning categorical labels to the reconstructed geometry [17, 18, 29, 46, 47]. Yet, these semantic approaches have relied on a closed-set paradigm, limiting them to predefined object labels. While the 3D reconstruction field is rapidly advancing towards open-vocabulary representations that can interpret arbitrary language queries [13, 19, 26, 44], integrating these capabilities into SLAM remains a challenge, due to critical limitations in real-time performance and model adaptability.

To address these limitations, we propose LEGO-SLAM (Language-Embedded Gaussian Optimization SLAM), the first framework that achieves real-time, open-vocabulary mapping within a Gaussian Splatting-based SLAM system. Approaches with open-vocabulary 3D reconstruction that store high-dimensional language features on each Gaussian are incompatible with the demands of SLAM. They suffer from rendering latency and high memory overhead, making them impractical for real-time applications [13, 19, 44]. Furthermore, methods that rely on pretrained models to extract fixed, low-dimensional features lack the adaptability required for SLAM systems, which must continuously learn from new environments [26]. Our core contribution overcomes these limitations by introducing a scene-adaptive autoencoder that distills high-dimensional language embeddings into a compact 16-dimensional feature space. This encoder trains in real-time to map visual information to a compact feature space, enabling highly efficient open-vocabulary 3D object localization. This is because instead of decoding the entire map back to a high-dimensional space for querying, we leverage the encoder to project the text query down into the map’s compact space for direct and

fast comparison. Specifically, we reduce the language feature dimension to 16, a choice that provides the optimal balance, as validated in Sec. 4.3, between minimizing memory per Gaussian and accelerating rendering. However, this compact 16-dimensional representation introduces an initialization challenge, as these abstract features cannot be derived from input RGB-D. We solve this by leveraging a pretrained encoder as a powerful prior, ensuring the rapid feature convergence essential for real-time SLAM.

Furthermore, the benefits of this compact 16-dimensional representation extend beyond mapping, allowing these features to be efficiently leveraged for other SLAM components. For instance, they enable an effective language-guided pruning strategy. By operating on the compact features, our system identifies semantically redundant Gaussians with negligible computational overhead, addressing the trade-offs of purely geometric pruning [7, 11, 12, 22, 45] without sacrificing important detail. In addition, these same mapping features are reused for loop detection. This integrated approach, which performs place recognition directly on our compact features, eliminates the need for separate, computationally expensive detection models [1, 24]. This ensures robust long-term drift correction and maintains tracking accuracy competitive with leading systems [20, 45], all without incurring additional overhead. We demonstrate the effectiveness of our framework on standard benchmarks including Replica [35], TUM-RGBD [36] and ScanNet [4], and our main contributions are as follows:

- We propose LEGO-SLAM, the real-time, open-vocabulary 3DGS SLAM framework for simultaneous high-fidelity mapping and tracking.
- A lightweight, scene-adaptive autoencoder that learns a compact 16-dim language representation, using a pretrained prior for rapid convergence, enabling real-time low-overhead mapping and efficient 3D object localization directly in the compact space.
- A semantic-guided Gaussian pruning strategy enhancing memory efficiency by removing semantically redundant Gaussians without sacrificing structural detail.
- An efficient, language-based loop detection reusing mapping features, avoiding a separate model while ensuring robust long-term tracking accuracy.

## 2 Related work

**Neural Rendering SLAM.** Recent advancements in differentiable rendering have given rise to a new paradigm in SLAM, often termed Neural Rendering SLAM. These methods move beyond traditional geometric representations to build high-fidelity, photorealistic maps by optimizing a scene representation against input images [37]. Early works in this domain integrated NeRF [23] into the SLAM pipeline, demonstrating the ability to construct continuous implicit map representations from RGB images [9, 20, 30, 42, 48]. While they produced maps of unprecedented visual quality, their high computational cost for per-ray rendering made them unsuitable for live SLAM operations. To address this bottleneck, 3DGS [12] marked a significant breakthrough. Its explicit representation

enables real-time rendering, leading to its rapid adoption in SLAM [11, 22, 38, 41]. Efforts have also aimed to improve long-term robustness in large-scale environments by incorporating loop closure into these systems [45]. While visually impressive, these photorealistic maps lack the semantic context required for meaningful robotic interaction. Consequently, the ambition of these systems has naturally evolved beyond photorealism towards semantic understanding. However, these efforts have predominantly operated within a closed-set paradigm, capable of recognizing only a predefined list of object categories [17, 18, 29, 46, 47].

**Open Vocabulary Scene Representation.** The transition to an interactive open-vocabulary map remains a significant hurdle for SLAM. Embedding the required high-dimensional language features introduces substantial memory and computational overhead [13, 19, 44]. Furthermore, reliance on static pre-trained models fundamentally conflict with the need for SLAM systems to continuously adapt to novel environments [26]. The foundation for this open-vocabulary shift was laid by powerful vision-language models, most notably CLIP [27], which learned a shared embedding space for images and text. Concurrently, powerful foundation models like DINO [2, 25] and the Segment Anything Model [14] emerged, demonstrating remarkable capabilities in tasks such as segmentation and tracking [3, 21, 28, 39], though they lack inherent open-vocabulary semantic recognition. Subsequent methods unlocked the ability to extract dense, per-pixel language features [6, 16], enabling a new class of open-vocabulary downstream tasks. These pixel-level language descriptors, combined with CLIP’s global understanding, have enabled lifting these features into 3D, leading to impressive open-vocabulary 3D reconstruction methods. However, they were not designed for the strict real-time constraints of SLAM, as distilling these high-dimensional features per-frame remains a significant bottleneck [13, 19, 26, 44]. In contrast, our work aims to bridge this gap by learning a compact and scene-adaptive language representation directly within a real-time SLAM framework.

### 3 Method

Our work, LEGO-SLAM, is the real-time system that constructs a 3D Gaussian Splatting map enriched with open-vocabulary language features. As illustrated in Fig. 2, our system integrates a Tracking module (Sec. 3.1) and the Mapping module (Sec. 3.2), which is responsible for optimizing the language-embedded map and enables downstream tasks such as 3D Object Localization. These are complemented by a Language Pruning strategy for efficient map management (Sec. 3.3) and a Loop Detection mechanism for long-term consistency (Sec. 3.4).

#### 3.1 Tracking

The tracking module estimates the camera pose  $T_k \in SE(3)$  for each incoming RGB-D frame  $I_k$ . Instead of costly photometric alignment, we adopt a direct 3D-to-3D geometric approach using the G-ICP algorithm [31]. A key advantage

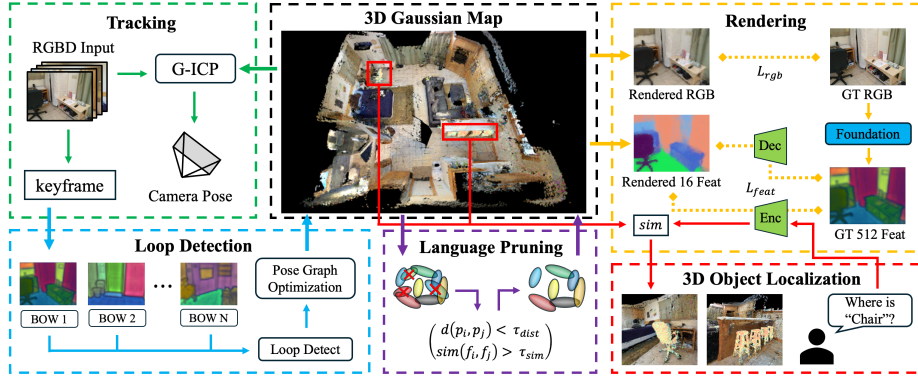


**Fig. 2: System Overview.** LEGO-SLAM architecture, where the Tracking module estimates pose and the Mapping module optimizes the 3D Gaussian Map via language distillation. This map is refined by Language Pruning and Loop Detection, enabling 3D Object Localization.

is that we directly track against our unified 3D Gaussian map, eliminating the need for a separate tracking map as seen in decoupled systems [24].

**Pose Estimation.** We estimate the camera pose  $T_k$  using G-ICP refinement [31], initializing the current pose with the previous optimized pose  $T_{k-1}$ . Source Gaussians are generated from the current depth image, while target Gaussians are sampled directly from our language-embedded 3DGS map. A key efficiency of our system is that the source covariances computed during tracking are reused to initialize new Gaussians in the mapping stage, avoiding redundant computations.

**Keyframe Selection.** After optimizing the pose, we select a frame as a keyframe if the proportion of inlier correspondences from the G-ICP alignment drops below a predefined threshold. This ensures new keyframes are added only when significant new information is observed.

### 3.2 Mapping

**Language-Embedded 3D Gaussians.** To enable open-vocabulary capabilities, we extend the standard 3D Gaussian representation. Each Gaussian is defined by a set of optimizable attributes  $\Theta = \{\mathbf{p}, \mathbf{q}, \mathbf{s}, \alpha, \mathbf{c}, \mathbf{f}\}$ , which includes position  $\mathbf{p}$ , rotation  $\mathbf{q}$ , scale  $\mathbf{s}$ , opacity  $\alpha$ , SH color coefficients  $\mathbf{c}$ , and crucially, our compact language feature  $\mathbf{f} \in \mathbb{R}^{16}$ . Following the standard 3DGS pipeline, these attributes are rendered to produce both an RGB image  $\hat{I}$  and a compact 16-dimensional feature map  $F_{\text{render}}$ .

**Gaussian Initialization.** When a new keyframe is received, we generate new 3D Gaussians from its depth data, deriving their geometric attributes of position, scale, and rotation from the 3D point cloud. Crucially, to maximize efficiency, we reuse the covariance matrices computed during the G-ICP tracking stage as the initial scale and rotation for these new Gaussians, avoiding redundant calculations.

While geometric properties are directly initialized, the abstract 16-dimensional language features present a unique challenge. To address this, we leverage our scene-adaptive encoder. We first use a pretrained 2D foundation model to extract a high-dimensional feature map from the keyframe’s RGB, which is then passed through our encoder to produce a strong prior for the new 16D features. This encoder-based initialization is critical for achieving the rapid feature convergence essential for real-time SLAM, as the encoder continuously adapts to the scene, providing a scene-specific prior for new Gaussians.

**Map Optimization via Feature Distillation.** Following initialization, we optimize the map over several iterations. In each iteration, we randomly select a keyframe from the active window to render its view and minimize a joint loss function  $\mathcal{L}_{\text{total}}$ :

$$\mathcal{L}_{\text{total}} = \mathcal{L}_{\text{rgb}} + w_{\text{depth}} \mathcal{L}_{\text{depth}} + w_{\text{feat}} \mathcal{L}_{\text{feat}} \quad (1)$$

where  $w_{\text{depth}}$  and  $w_{\text{feat}}$  are weighting coefficients. The photometric loss  $\mathcal{L}_{\text{rgb}}$  combines an L1 and a D-SSIM term between the rendered  $\hat{I}$  and ground-truth  $I$ . The geometric loss  $\mathcal{L}_{\text{depth}}$  is an L1 loss between the rendered  $\hat{D}$  and ground-truth  $D$ . The feature distillation loss  $\mathcal{L}_{\text{feat}}$  is the core of our language feature learning:

$$\mathcal{L}_{\text{feat}} = \mathcal{L}_{\text{L1}}(D_{\theta}(F_{\text{render}}), F_{gt}) \quad (2)$$

To compute this, we render the compact 16-dimensional feature map  $F_{\text{render}}$  from our 3D Gaussians. This map is passed through our lightweight convolutional decoder  $D_{\theta}$  to upsample it to the high dimension, such as 512D, of the frozen guidance model’s features  $F_{gt}$  for L1 comparison. This distillation process allows our 3D Gaussians to learn a compact and scene-adaptive language representation while maintaining real-time performance.

**Scene-Adaptive Encoder Optimization.** We found that jointly optimizing the encoder  $E_{\phi}$  with the map introduces training instability, especially if adaptation starts before the Gaussian features  $\mathbf{f}$  converge. Therefore, we adopt a decoupled strategy, freezing  $E_{\phi}$  during the initial map optimization to allow  $\mathbf{f}$  to stabilize first. After feature convergence, we periodically adapt  $E_{\phi}$  by freezing the map and decoder  $D_{\theta}$  and minimizing only  $\mathcal{L}_{\text{enc}}$ :

$$\mathcal{L}_{\text{enc}} = \mathcal{L}_{\text{L1}}(E_{\phi}(F_{gt}), F_{\text{render}}) \quad (3)$$

This trains  $E_{\phi}$  to map the high-dimensional  $F_{gt}$  to the map’s learned  $F_{\text{render}}$ , ensuring stable convergence. This adaptive encoder is critical for real-time 3D object localization, as shown in Sec. 4.3.

### 3.3 Language-Guided Gaussian Pruning

To maintain map efficiency and compactness, we periodically prune Gaussians. Conventional pruning in 3DGS-based systems [7, 11, 12, 45] relies on geometric heuristics, such as low opacity or large scale. However, these methods struggle to distinguish redundant Gaussians, and aggressive geometric pruning often degrades map quality by removing structurally important primitives.

To overcome this, we introduce a language-guided pruning strategy that augments the geometric criteria with a semantic one, identifying redundant Gaussians that are both spatially proximate and semantically similar. This check is highly efficient as it operates directly on the compact 16-dimensional language features  $\mathbf{f}$  already stored on each Gaussian. This eliminates the need for additional feature extraction, in contrast to other semantic pruning methods that require separate models or significant overhead [8, 40, 43].

Specifically, our method identifies redundant primitives by evaluating each Gaussian  $G_i$  against its local neighborhood. We first find its K-nearest neighbors in 3D space. Then, for each neighbor  $G_j$ , we evaluate its redundancy based on both its Euclidean distance  $d(\mathbf{p}_i, \mathbf{p}_j)$  and the cosine similarity of their language features,  $\text{sim}(\mathbf{f}_i, \mathbf{f}_j)$ . A neighbor  $G_j$  is marked as redundant if it satisfies the following condition:

$$(d(\mathbf{p}_i, \mathbf{p}_j) < \tau_{dist}) \wedge (\text{sim}(\mathbf{f}_i, \mathbf{f}_j) > \tau_{sim}) \quad (4)$$

where  $\tau_{dist}$  and  $\tau_{sim}$  are predefined distance and similarity thresholds. The final set of Gaussians to be pruned is the union of those identified by our language-based redundancy check and those filtered by the traditional geometric criteria.

### 3.4 Language-Based Loop Closure

To correct the inevitable drift accumulated during long-term operation, we incorporate a language-based loop closure module. Our approach is designed for high efficiency by reusing the features already computed for mapping, avoiding separate loop detection models [1, 24].

**Language-Based Candidate Detection.** Our approach performs place recognition by representing each keyframe with a compact semantic signature. This uses a language codebook, generated offline by applying k-means clustering to high-dimensional language features. This vocabulary allows us to create a normalized histogram for each new keyframe by assigning its pixel features to the closest clusters in the codebook. To find potential loop candidates, we compute the cosine similarity between the current keyframe’s histogram and those of spatially proximate past keyframes. Keyframes with a similarity above a threshold  $\tau_{sim}$  are selected as potential loop candidates.

**Geometric Verification and Global Optimization.** Each loop candidate undergoes a rigorous geometric verification using G-ICP against a local submap. If a match is confirmed based on overlap and RMSE thresholds, its relative pose transformation  $\mathbf{T}_{ij}$  is added as a constraint to a pose graph. We then employ GSTAM [5] to optimize the entire trajectory for global consistency, propagating the corrected poses back to our 3D Gaussian map.

## 4 Experiments

### 4.1 Experiments Setup

**Datasets and Metrics.** We evaluate our framework on three datasets, including the synthetic Replica dataset [35], and the real-world TUM-RGBD [36] and

ScanNet [4] datasets. For tables that report a single metric per dataset, the value represents the average performance across all evaluated scenes. Tracking Accuracy is evaluated using Absolute Trajectory Error (ATE RMSE [cm]). Mapping quality is assessed via PSNR, SSIM, and LPIPS. For open-vocabulary performance, we measure semantic understanding using mean Intersection-over-Union (mIoU) and pixel-wise Accuracy, following the protocol of Feature 3DGS [44].

**Implementation Details.** All experiments are conducted on a desktop with a Ryzen 7 7800x3d CPU, 32GB RAM, and an NVIDIA RTX 4090 GPU. The ground-truth feature maps for distillation are pre-distilled by extracting per-pixel language embeddings using LSeg [16]. Our scene-adaptive encoder and decoder, composed of lightweight 1x1 convolutional layers, are pretrained as an autoencoder to learn the compression to our 16-dimensional space. The language codebook for loop closure is generated offline via k-means clustering ( $k=64$ ) on millions of feature vectors. During the SLAM process, our language-guided pruning is performed every 200 iterations, and for loop detection, we select the top two candidates with a cosine similarity above 0.7 for geometric verification. Crucially, to reflect true online performance, all evaluations are performed on the final map generated during the SLAM process, without any post-run optimization iterations.

**Baseline.** We evaluate LEGO-SLAM against baselines, with all methods run on the same hardware. For open-vocabulary performance, we compare against LeRF [13], LangSplat [26], and Feature 3DGS [44]. For core SLAM capabilities, we benchmark against NeRF-based systems (NICE-SLAM [48], Point-SLAM [30], Loopy-SLAM [20]) and 3DGS-based systems (MonoGS [22], SplatAM [11], LoopSplat [45]), including those that incorporate loop closure mechanisms.

## 4.2 Quantitative Evaluation

**Table 1: Open-Vocabulary Segmentation on 3 datasets.** LEGO-SLAM uses estimated poses while baselines use GT poses. Feature 3DGS with 512-dim features failed on several scenes due to memory constraints, unlike our compact 16-dim features.

Method	Metrics	Replica	TUM-RGBD	ScanNet
LeRF [13]	Accuracy $\uparrow$	0.617	0.490	0.261
	mIoU $\uparrow$	0.276	0.263	0.066
LangSplat [26]	Accuracy $\uparrow$	0.614	0.544	0.429
	mIoU $\uparrow$	0.263	0.229	0.160
Feature 3DGS [44]	Accuracy $\uparrow$	0.902	0.835	fail
	mIoU $\uparrow$	0.691	0.633	fail
LEGO-SLAM	Accuracy $\uparrow$	0.882	0.834	0.791
	mIoU $\uparrow$	0.674	0.650	0.519

**Open-Vocabulary Performance.** We evaluate the open-vocabulary mapping performance of LEGO-SLAM against leading 3D reconstruction methods, with results summarized in Tab. 1. For this evaluation, we follow the protocol of [44] and use the per-pixel language embeddings extracted by LSeg [16] as the GT features for all methods. To ensure a fair comparison, we trained all baseline reconstruction methods for 3000 iterations, aligning with the optimization steps available to our mapping module. Feature 3DGS [44] achieves high accuracy on Replica by distilling full 512-dimensional features but suffers from significant memory overhead, causing it to fail on larger-scale ScanNet scenes. Conversely, LangSplat [26] compresses features to only 3 dimensions, which substantially reduces memory but also leads to significantly lower semantic accuracy. LEGO-SLAM achieves a strong balance, delivering performance competitive with Feature 3DGS on Replica while successfully scaling to all large-scale ScanNet scenes where memory-intensive methods fail. Notably, these results are achieved even though LEGO-SLAM learns concurrently from estimated camera poses, a more challenging and realistic setting compared to the ground-truth poses used by all baseline methods.

**Tracking Accuracy.** We evaluate the tracking accuracy of LEGO-SLAM against prominent NeRF-based and 3DGS-based SLAM systems (Tabs. 2 to 4). On the Replica dataset, LEGO-SLAM achieves the lowest average ATE (0.20 cm). It remains competitive on the challenging real-world TUM-RGBD sequences (2.30 cm) and large-scale ScanNet (8.68 cm). This ScanNet performance, which leverages our efficient language-based loop closure, is comparable to specialized loop-closure systems like LoopSplat and Loopy-SLAM, while achieving higher accuracy than non-loop-closure baselines. Crucially, this high accuracy is achieved at a consistent 15 FPS (Tab. 5), operating faster than competitors. Notably, this competitive tracking performance is achieved while LEGO-SLAM concurrently builds a rich, open-vocabulary map, whereas the compared baselines only perform geometric and RGB mapping.

**Table 2: Tracking Performance on Replica [35]** (ATE RMSE [cm]  $\downarrow$ ). The best results are highlighted as **first**, **second**, and **third**.

Method	R0	R1	R2	O0	O1	O2	O3	O4	Avg.
NICE-SLAM [48]	0.97	1.31	1.07	0.88	1.00	1.06	1.10	1.13	1.06
Point-SLAM [30]	0.54	0.41	<b>0.23</b>	0.32	0.45	0.48	0.56	0.68	0.47
Loopy-SLAM [20]	<b>0.30</b>	0.47	0.30	<b>0.25</b>	<b>0.21</b>	0.31	0.32	<b>0.40</b>	0.32
MonoGS [22]	<b>0.30</b>	<b>0.22</b>	0.28	0.36	<b>0.21</b>	<b>0.24</b>	<b>0.12</b>	0.77	<b>0.31</b>
SplatAM [11]	0.31	0.39	0.27	0.49	0.23	0.30	0.32	0.60	0.36
LoopSplat [45]	0.27	0.24	<b>0.16</b>	0.23	0.17	0.36	0.21	0.36	0.25
LEGO-SLAM	<b>0.15</b>	<b>0.21</b>	<b>0.16</b>	<b>0.20</b>	<b>0.16</b>	<b>0.22</b>	0.28	<b>0.22</b>	<b>0.20</b>

**Table 3: Tracking Performance on TUM-RGBD [36] (ATE RMSE [cm] ↓).**

Method	fr1-desk	fr2-xyz	fr3-office	Avg.
NICE-SLAM [48]	2.80	2.10	7.20	4.00
Point-SLAM [30]	2.73	<b>1.30</b>	3.51	2.51
Loopy-SLAM [20]	3.74	1.90	3.12	2.92
MonoGS [22]	<b>1.47</b>	1.57	<b>1.51</b>	<b>1.51</b>
SplaTAM [11]	3.31	1.35	5.13	3.26
LoopSplat [45]	2.35	1.41	3.90	2.55
LEGO-SLAM	2.53	1.72	2.64	2.30

**Table 4: Tracking Performance on ScanNet [4] (ATE RMSE [cm] ↓).**

Method	00	59	106	169	181	207	Avg.
NICE-SLAM [48]	12.0	14.0	<b>7.9</b>	10.9	13.4	6.2	10.73
Point-SLAM [30]	9.60	<b>7.24</b>	8.44	20.92	14.41	<b>4.56</b>	10.86
Loopy-SLAM [20]	<b>4.63</b>	7.82	8.55	<b>7.97</b>	11.65	6.59	<b>7.87</b>
MonoGS [22]	30.34	17.03	11.30	21.53	20.51	8.07	18.13
SplaTAM [11]	12.19	10.01	18.05	12.37	12.78	7.74	12.19
LoopSplat [45]	5.30	<b>7.09</b>	<b>6.54</b>	10.76	<b>7.93</b>	6.07	<b>7.28</b>
LEGO-SLAM	5.78	13.43	7.58	<b>6.47</b>	12.68	6.11	8.68

**Mapping Quality and FPS.** We evaluate the mapping quality and system speed in Tab. 5. LEGO-SLAM achieves high-fidelity mapping quality while building a rich, open-vocabulary map at 15 FPS. Across all datasets, our method demonstrates leading performance in mapping quality results against all baselines. All metrics are from the online SLAM process without post-run optimization. This 15 FPS operation is significantly faster than all competing Neural Rendering SLAM systems in the table, which operate at non-real-time rates.



**Fig. 3: Qualitative Mapping Comparison.** We compare the rendered maps of LEGO-SLAM against baselines on the TUM-RGBD, and ScanNet datasets. All maps shown are captured directly from the online SLAM process without any post-run optimization.

**Table 5: Rendering Performance and FPS on 3 datasets.** All metrics are from the online SLAM process without post-run optimization. LEGO-SLAM achieves high-fidelity rendering quality at 15 FPS, operating faster than all baselines.

Method	Metrics	Replica	TUM-RGBD	ScanNet
Point-SLAM [30]	PSNR[dB] $\uparrow$	35.56	21.33	<b>23.31</b>
	SSIM $\uparrow$	<b>0.977</b>	0.733	0.753
	LPIPS $\downarrow$	0.118	0.453	0.509
	FPS $\uparrow$	0.415	0.252	0.233
Loopy-SLAM [20]	PSNR[dB] $\uparrow$	19.28	14.32	12.46
	SSIM $\uparrow$	0.662	0.512	0.495
	LPIPS $\downarrow$	0.506	0.470	0.574
	FPS $\uparrow$	0.374	0.222	0.357
MonoGS [22]	PSNR[dB] $\uparrow$	<b>35.33</b>	17.82	16.23
	SSIM $\uparrow$	0.943	0.714	0.599
	LPIPS $\downarrow$	0.122	<b>0.327</b>	0.588
	FPS $\uparrow$	<b>0.679</b>	2.52	<b>2.01</b>
SplaTAM [11]	PSNR[dB] $\uparrow$	34.19	23.53	18.82
	SSIM $\uparrow$	<b>0.970</b>	<b>0.908</b>	0.699
	LPIPS $\downarrow$	0.094	0.166	0.370
	FPS $\uparrow$	0.212	0.407	0.544
LoopSplat [45]	PSNR[dB] $\uparrow$	14.13	12.85	14.20
	SSIM $\uparrow$	0.748	0.511	0.571
	LPIPS $\downarrow$	0.584	0.746	0.708
	FPS $\uparrow$	<b>0.651</b>	0.58	<b>0.445</b>
LEGO-SLAM	PSNR[dB] $\uparrow$	<b>36.38</b>	<b>23.86</b>	19.44
	SSIM $\uparrow$	0.957	0.858	<b>0.758</b>
	LPIPS $\downarrow$	<b>0.075</b>	<b>0.138</b>	<b>0.286</b>
	FPS $\uparrow$	<b>15.0</b>	<b>15.0</b>	<b>15.0</b>

### 4.3 Ablation Study

**Analysis of the Scene-Adaptive Encoder.** We validate our encoder-based initialization strategy, which is essential for real-time SLAM systems that must continuously adapt to new environments. As shown in Tab. 6, training from scratch (Ours w/o Init) requires a high number of iterations for the abstract feature loss to converge. In contrast, by using our pretrained encoder to provide a strong prior for new Gaussians (Ours w/ Init), the feature convergence is considerably accelerated.

Furthermore, our scene-adaptive encoder design provides a second, equally important advantage by enabling efficient 3D object localization. Rather than decoding the entire map back to a high-dimensional space for querying, we leverage the learned encoder to project the text query directly into the map’s compact 16-dimensional space for fast, direct comparison. While pretraining provides a strong start, continuous adaptation is critical in SLAM, where systems must

learn from new environments, unlike methods that rely on static feature extractors. To demonstrate this necessity, we compare our adaptive encoder against a baseline where the pretrained encoder is kept frozen. As visualized in Fig. 4, the frozen encoder fails to produce meaningful localization results, as its static features cannot adapt to the specific scene. Our scene-adaptive encoder, however, successfully localizes the object, proving that continuous online learning is critical for our system’s emergent open-vocabulary capabilities.

**Table 6: Ablation on Initialization.** Convergence speed in iterations comparing pretrained initialization against training from scratch (Convergence thresholds: Total  $< 0.1$ , RGB  $< 0.05$ , Feature  $< 0.05$ ).

Method	Conv. Steps	Replica	TUM-RGBD	ScanNet
Ours (w/o Init)	RGB	<b>214</b>	<b>238</b>	288
	Feature	228	230	228
	Total	219	232	247
Ours (w/ Init)	RGB	<b>214</b>	240	<b>277</b>
	Feature	<b>76</b>	<b>54</b>	<b>67</b>
	Total	<b>179</b>	<b>145</b>	<b>154</b>



**Fig. 4: Scene-Adaptive Encoder Adaptation.** Our Adaptive, online-tuned encoder generates accurate relevancy maps for 3D object queries, while the Frozen baseline fails.

**Impact of Feature Dimension.** We investigate the impact of our compact feature dimension ( $d$ ) on mapping quality, semantic accuracy, and memory usage in Tab. 7. Selecting the feature dimension involves a critical trade-off. A larger  $d$  increases memory and rendering costs, which in turn reduces the mapping optimization iterations available in real-time SLAM. This trade-off is clear at the extremes. At  $d = 8$ , the system is most efficient, yielding the highest PSNR as geometry converges more fully. However, its semantic accuracy is lowest, as 8 dimensions are insufficient for feature reconstruction. Conversely, at

**Table 7: Ablation study on the impact of feature dimension (d).**

Method	Metrics	Replica	TUM-RGBD	ScanNet
Ours (d=8)	PSNR [dB] $\uparrow$	<b>36.61</b>	<b>24.07</b>	<b>19.49</b>
	Accuracy $\uparrow$	0.854	0.784	0.746
	Memory [MB] $\downarrow$	<b>61.9</b>	<b>71.5</b>	<b>194.6</b>
Ours (d=16)	PSNR [dB] $\uparrow$	36.38	23.86	19.44
	Accuracy $\uparrow$	<b>0.882</b>	<b>0.834</b>	<b>0.791</b>
	Memory [MB] $\downarrow$	81.8	92.9	256.6
Ours (d=32)	PSNR [dB] $\uparrow$	35.84	23.38	19.24
	Accuracy $\uparrow$	0.861	0.816	0.776
	Memory [MB] $\downarrow$	123.7	146.1	385.6
Ours (d=64)	PSNR [dB] $\uparrow$	34.93	23.00	19.16
	Accuracy $\uparrow$	0.861	0.810	0.778
	Memory [MB] $\downarrow$	123.7	248.1	636.6
Ours (d=128)	PSNR [dB] $\uparrow$	32.86	22.34	fail
	Accuracy $\uparrow$	0.771	0.795	fail
	Memory [MB] $\downarrow$	371.1	452.7	fail

$d \geq 32$ , semantic accuracy also drops because slower rendering reduces mapping iterations, preventing feature convergence. At  $d = 128$ , the memory overhead is prohibitive, failing on ScanNet. Based on this analysis, we select  $d = 16$ . This choice represents an intentional trade-off for robust language alignment. As validated in Tab. 7, we accept a minor sacrifice in geometric quality, seen as a slight PSNR drop compared to  $d = 8$ , to gain a significant improvement in semantic accuracy. This trade-off allows us to balance the crucial demands of language representation power with the low memory essential for real-time SLAM.

**Analysis of Language-Guided Pruning.** We analyze the effectiveness of our language-guided pruning against the conventional geometry-based pruning used in systems [11,45]. To test robustness, we compare their performance as the pruning aggressiveness is increased. As visualized in Fig. 5, the geometric approach’s rendering quality degrades sharply even at low pruning ratios, leading to a severe

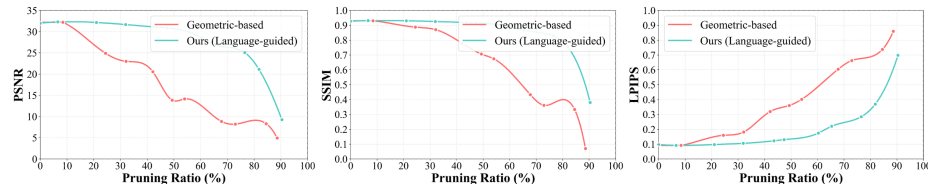


**Fig. 5: Pruning Performance Comparison.** As the pruning ratio increases, our language-guided method shows significantly less degradation in rendering quality compared to the geometric approach on the Replica Room0 scene.

degradation as aggressiveness increases. In contrast, our language-guided method remains robust, maintaining high rendering quality across a much wider range of pruning ratios. This stability is confirmed by Tab. 8, which shows that at a highly aggressive pruning level, our method maintains high PSNR and semantic accuracy where the geometric-only strategy fails. This effectiveness is achieved with negligible computational overhead, as our semantic check efficiently reuses the compact 16-dimensional features already stored on the Gaussians.

**Table 8: Pruning Ablation Study.** We compare our language-guided strategy against a geometric-only baseline under a highly aggressive setting.

Method	Metrics	Replica	TUM-RGBD	ScanNet
Baseline (No Pruning)	PSNR $\uparrow$	36.14	23.80	19.25
	SSIM $\uparrow$	0.956	0.857	0.753
	LPIPS $\downarrow$	0.077	0.137	0.294
	Acc $\uparrow$	0.880	0.833	0.788
	IoU $\uparrow$	0.649	0.647	0.515
	# of GS (K) $\downarrow$	645	761	2063
Baseline [11, 45] (Geo Pruning)	PSNR $\uparrow$	24.20	17.39	16.56
	SSIM $\uparrow$	0.833	0.725	0.655
	LPIPS $\downarrow$	0.232	0.281	0.377
	Acc $\uparrow$	0.834	0.772	0.725
	IoU $\uparrow$	0.574	0.570	0.451
	# of GS (K) $\downarrow$	400	232	951
Ours (Lang Pruning)	PSNR $\uparrow$	<b>35.21</b>	<b>22.34</b>	<b>19.16</b>
	SSIM $\uparrow$	<b>0.949</b>	<b>0.820</b>	<b>0.753</b>
	LPIPS $\downarrow$	<b>0.098</b>	<b>0.191</b>	<b>0.298</b>
	Acc $\uparrow$	<b>0.880</b>	<b>0.819</b>	<b>0.786</b>
	IoU $\uparrow$	<b>0.649</b>	<b>0.632</b>	<b>0.516</b>
	# of GS (K) $\downarrow$	<b>382</b>	<b>218</b>	<b>928</b>

**Effectiveness of Language-Based Loop Detection.** We validate our integrated language-based loop closure module. It is efficient as it directly reuses language features computed during the mapping process, avoiding the computational overhead of separate models [1, 24] that would compromise our real-time objective. To demonstrate this efficiency does not sacrifice accuracy, we there-

**Table 9: Loop Detection Comparison.** Our language-based method achieves lower tracking error (ATE RMSE [cm]  $\downarrow$ ) than the position-based approach.

Method	Replica	TUM-RGBD	ScanNet
Position-based [34]	0.276	3.06	10.15
Language-based	<b>0.206</b>	<b>2.30</b>	<b>8.68</b>

fore compare its performance against a similarly lightweight, real-time position-based baseline [34]. As shown in Tab. 9, our language-based method consistently achieves a lower tracking error across all datasets. This confirms it offers more robust place recognition than the position-based approach.

## 5 Conclusion

We proposed LEGO-SLAM, the first real-time, open-vocabulary 3DGS SLAM system. Our core contribution is a lightweight, scene-adaptive autoencoder that distills language features into a compact 16-dimensional space, considerably reducing memory and rendering overhead to enable real-time performance. These features also enhance the SLAM pipeline by enabling a language-guided pruning strategy and an efficient feature-reuse loop closure. Experiments demonstrated that LEGO-SLAM achieves competitive mapping quality and tracking accuracy at real-time speeds.

## References

1. Arandjelovic, R., Gronat, P., Torii, A., Pajdla, T., Sivic, J.: Netvlad: Cnn architecture for weakly supervised place recognition. In: Proceedings of the IEEE conference on computer vision and pattern recognition. pp. 5297–5307 (2016)
2. Caron, M., Touvron, H., Misra, I., Jégou, H., Mairal, J., Bojanowski, P., Joulin, A.: Emerging properties in self-supervised vision transformers. In: Proceedings of the IEEE/CVF international conference on computer vision. pp. 9650–9660 (2021)
3. Cheng, H.K., Oh, S.W., Price, B., Schwing, A., Lee, J.Y.: Tracking anything with decoupled video segmentation. In: Proceedings of the IEEE/CVF International Conference on Computer Vision. pp. 1316–1326 (2023)
4. Dai, A., Chang, A.X., Savva, M., Halber, M., Funkhouser, T., Nießner, M.: Scannet: Richly-annotated 3d reconstructions of indoor scenes. In: Proceedings of the IEEE conference on computer vision and pattern recognition. pp. 5828–5839 (2017)
5. Dellaert, F.: Factor graphs and gtsam: A hands-on introduction. Georgia Institute of Technology, Tech. Rep **2**(4) (2012)
6. Ghiasi, G., Gu, X., Cui, Y., Lin, T.Y.: Scaling open-vocabulary image segmentation with image-level labels. In: European conference on computer vision. pp. 540–557. Springer (2022)
7. Ha, S., Yeon, J., Yu, H.: Rgbd gs-icp slam. In: European Conference on Computer Vision. pp. 180–197. Springer (2024)
8. Hanson, A., Tu, A., Singla, V., Jayawardhana, M., Zwicker, M., Goldstein, T.: Pup 3d-gs: Principled uncertainty pruning for 3d gaussian splatting. In: Proceedings of the Computer Vision and Pattern Recognition Conference. pp. 5949–5958 (2025)
9. Johari, M.M., Carta, C., Fleuret, F.: Eslam: Efficient dense slam system based on hybrid representation of signed distance fields. In: Proceedings of the IEEE/CVF conference on computer vision and pattern recognition. pp. 17408–17419 (2023)
10. Kant, Y., Ramachandran, A., Yenamandra, S., Gilitschenski, I., Batra, D., Szot, A., Agrawal, H.: Housekeep: Tidying virtual households using commonsense reasoning. In: European Conference on Computer Vision. pp. 355–373. Springer (2022)

11. Keetha, N., Karhade, J., Jatavallabhula, K.M., Yang, G., Scherer, S., Ramanan, D., Luiten, J.: Splatam: Splat track & map 3d gaussians for dense rgb-d slam. In: Proceedings of the IEEE/CVF Conference on Computer Vision and Pattern Recognition. pp. 21357–21366 (2024)
12. Kerbl, B., Kopanas, G., Leimkühler, T., Drettakis, G.: 3d gaussian splatting for real-time radiance field rendering. *ACM Trans. Graph.* **42**(4), 139–1 (2023)
13. Kerr, J., Kim, C.M., Goldberg, K., Kanazawa, A., Tancik, M.: Lerf: Language embedded radiance fields. In: Proceedings of the IEEE/CVF international conference on computer vision. pp. 19729–19739 (2023)
14. Kirillov, A., Mintun, E., Ravi, N., Mao, H., Rolland, C., Gustafson, L., Xiao, T., Whitehead, S., Berg, A.C., Lo, W.Y., et al.: Segment anything. In: Proceedings of the IEEE/CVF international conference on computer vision. pp. 4015–4026 (2023)
15. Lee, S., Yu, H., Kim, G., Choi, S.: Lamp: Implicit language map for robot navigation. *IEEE Robotics and Automation Letters* (2025)
16. Li, B., Weinberger, K.Q., Belongie, S., Koltun, V., Ranftl, R.: Language-driven semantic segmentation. arXiv preprint arXiv:2201.03546 (2022)
17. Li, K., Niemeyer, M., Navab, N., Tombari, F.: Dns-slam: Dense neural semantic-informed slam. In: 2024 IEEE/RSJ International Conference on Intelligent Robots and Systems (IROS). pp. 7839–7846. IEEE (2024)
18. Li, M., Liu, S., Zhou, H., Zhu, G., Cheng, N., Deng, T., Wang, H.: Sgs-slam: Semantic gaussian splatting for neural dense slam. In: European Conference on Computer Vision. pp. 163–179. Springer (2024)
19. Liao, G., Zhou, K., Bao, Z., Liu, K., Li, Q.: Ov-nerf: Open-vocabulary neural radiance fields with vision and language foundation models for 3d semantic understanding. *IEEE Transactions on Circuits and Systems for Video Technology* (2024)
20. Liso, L., Sandström, E., Yugay, V., Van Gool, L., Oswald, M.R.: Loopy-slam: Dense neural slam with loop closures. In: Proceedings of the IEEE/CVF conference on computer vision and pattern recognition. pp. 20363–20373 (2024)
21. Liu, S., Zeng, Z., Ren, T., Li, F., Zhang, H., Yang, J., Jiang, Q., Li, C., Yang, J., Su, H., et al.: Grounding dino: Marrying dino with grounded pre-training for open-set object detection. In: European conference on computer vision. pp. 38–55. Springer (2024)
22. Matsuki, H., Murai, R., Kelly, P.H., Davison, A.J.: Gaussian splatting slam. In: Proceedings of the IEEE/CVF Conference on Computer Vision and Pattern Recognition. pp. 18039–18048 (2024)
23. Mildenhall, B., Srinivasan, P.P., Tancik, M., Barron, J.T., Ramamoorthi, R., Ng, R.: Nerf: Representing scenes as neural radiance fields for view synthesis. *Communications of the ACM* **65**(1), 99–106 (2021)
24. Mur-Artal, R., Tardós, J.D.: Orb-slam2: An open-source slam system for monocular, stereo, and rgb-d cameras. *IEEE transactions on robotics* **33**(5), 1255–1262 (2017)
25. Oquab, M., Darcet, T., Moutakanni, T., Vo, H., Szafraniec, M., Khalidov, V., Fernandez, P., Haziza, D., Massa, F., El-Nouby, A., et al.: Dinov2: Learning robust visual features without supervision. arXiv preprint arXiv:2304.07193 (2023)
26. Qin, M., Li, W., Zhou, J., Wang, H., Pfister, H.: Langsplat: 3d language gaussian splatting. In: Proceedings of the IEEE/CVF Conference on Computer Vision and Pattern Recognition. pp. 20051–20060 (2024)
27. Radford, A., Kim, J.W., Hallacy, C., Ramesh, A., Goh, G., Agarwal, S., Sastry, G., Askell, A., Mishkin, P., Clark, J., et al.: Learning transferable visual models from

natural language supervision. In: International conference on machine learning. pp. 8748–8763. PMLR (2021)

28. Ranftl, R., Bochkovskiy, A., Koltun, V.: Vision transformers for dense prediction. In: Proceedings of the IEEE/CVF international conference on computer vision. pp. 12179–12188 (2021)
29. Rosinol, A., Abate, M., Chang, Y., Carbone, L.: Kimera: an open-source library for real-time metric-semantic localization and mapping. In: 2020 IEEE International Conference on Robotics and Automation (ICRA). pp. 1689–1696. IEEE (2020)
30. Sandström, E., Li, Y., Van Gool, L., Oswald, M.R.: Point-slam: Dense neural point cloud-based slam. In: Proceedings of the IEEE/CVF International Conference on Computer Vision. pp. 18433–18444 (2023)
31. Segal, A., Haehnel, D., Thrun, S.: Generalized-icp. In: Robotics: science and systems. vol. 2, p. 435. Seattle, WA (2009)
32. Shafullah, N.M.M., Paxton, C., Pinto, L., Chintala, S., Szlam, A.: Clip-fields: Weakly supervised semantic fields for robotic memory. arXiv preprint arXiv:2210.05663 (2022)
33. Shah, D., Osiński, B., Levine, S., et al.: Lm-nav: Robotic navigation with large pre-trained models of language, vision, and action. In: Conference on robot learning. pp. 492–504. PMLR (2023)
34. Shan, T., Englot, B., Meyers, D., Wang, W., Ratti, C., Rus, D.: Lio-sam: Tightly-coupled lidar inertial odometry via smoothing and mapping. In: 2020 IEEE/RSJ international conference on intelligent robots and systems (IROS). pp. 5135–5142. IEEE (2020)
35. Straub, J., Whelan, T., Ma, L., Chen, Y., Wijmans, E., Green, S., Engel, J.J., Mur-Artal, R., Ren, C., Verma, S., et al.: The replica dataset: A digital replica of indoor spaces. arXiv preprint arXiv:1906.05797 (2019)
36. Sturm, J., Engelhard, N., Endres, F., Burgard, W., Cremers, D.: A benchmark for the evaluation of rgbd slam systems. In: 2012 IEEE/RSJ international conference on intelligent robots and systems. pp. 573–580. IEEE (2012)
37. Tosi, F., Zhang, Y., Gong, Z., Sandström, E., Mattoccia, S., Oswald, M.R., Poggi, M.: How nerfs and 3d gaussian splatting are reshaping slam: a survey. arXiv preprint arXiv:2402.13255 4, 1 (2024)
38. Yan, C., Qu, D., Xu, D., Zhao, B., Wang, Z., Wang, D., Li, X.: Gs-slam: Dense visual slam with 3d gaussian splatting. In: Proceedings of the IEEE/CVF Conference on Computer Vision and Pattern Recognition. pp. 19595–19604 (2024)
39. Yang, L., Kang, B., Huang, Z., Xu, X., Feng, J., Zhao, H.: Depth anything: Unleashing the power of large-scale unlabeled data. In: Proceedings of the IEEE/CVF conference on computer vision and pattern recognition. pp. 10371–10381 (2024)
40. Ye, Z., Wan, C., Li, C., Hong, J., Li, S., Li, L., Zhang, Y., Lin, Y.C.: 3d gaussian rendering can be sparser: Efficient rendering via learned fragment pruning. Advances in Neural Information Processing Systems **37**, 5850–5869 (2024)
41. Yugay, V., Li, Y., Gevers, T., Oswald, M.R.: Gaussian-slam: Photo-realistic dense slam with gaussian splatting. arXiv preprint arXiv:2312.10070 (2023)
42. Zhang, Y., Tosi, F., Mattoccia, S., Poggi, M.: Go-slam: Global optimization for consistent 3d instant reconstruction. In: Proceedings of the IEEE/CVF International Conference on Computer Vision. pp. 3727–3737 (2023)
43. Zhang, Z., Song, T., Lee, Y., Yang, L., Peng, C., Chellappa, R., Fan, D.: Lp-3dgs: Learning to prune 3d gaussian splatting. Advances in Neural Information Processing Systems **37**, 122434–122457 (2024)

44. Zhou, S., Chang, H., Jiang, S., Fan, Z., Zhu, Z., Xu, D., Chari, P., You, S., Wang, Z., Kadambi, A.: Feature 3dgs: Supercharging 3d gaussian splatting to enable distilled feature fields. In: Proceedings of the IEEE/CVF Conference on Computer Vision and Pattern Recognition. pp. 21676–21685 (2024)
45. Zhu, L., Li, Y., Sandström, E., Huang, S., Schindler, K., Armeni, I.: Loopsplat: Loop closure by registering 3d gaussian splats. In: 2025 International Conference on 3D Vision (3DV). pp. 156–167. IEEE (2025)
46. Zhu, S., Qin, R., Wang, G., Liu, J., Wang, H.: Semgauss-slam: Dense semantic gaussian splatting slam. arXiv preprint arXiv:2403.07494 (2024)
47. Zhu, S., Wang, G., Blum, H., Liu, J., Song, L., Pollefeys, M., Wang, H.: Sni-slam: Semantic neural implicit slam. In: Proceedings of the IEEE/CVF Conference on Computer Vision and Pattern Recognition. pp. 21167–21177 (2024)
48. Zhu, Z., Peng, S., Larsson, V., Xu, W., Bao, H., Cui, Z., Oswald, M.R., Pollefeys, M.: Nice-slam: Neural implicit scalable encoding for slam. In: Proceedings of the IEEE/CVF conference on computer vision and pattern recognition. pp. 12786–12796 (2022)